Inorganic Chemistry

pubs.acs.org/IC

Communication

Hemilabile Binding of Acetylene in an Amide-Rich Ultramicroporous MOF Enables Strong Acetylene Selectivity

Published as part of Inorganic Chemistry virtual special issue "Celebrating the 25th Anniversary of the Chemical Research Society of India".

Subhajit Dutta,[⊥] Soumya Mukherjee,[⊥] Sousa Javan Nikkhah, Omid T. Qazvini, Gourab K. Dam, Matthias Vandichel,* Tarak Nath Mandal,* and Sujit K. Ghosh*

Cite This: *Inorg. Chem.* 2024, 63, 12404−12408

Read Online

ACCESS | Metrics & More | Article Recommendations | Supporting Information

ABSTRACT: Thanks to a hemilabile amide-based binding site, a previously unreported amide-functionalized metal−organic framework (MOF) exhibits high acetylene affinity over ethylene, methane, and carbon dioxide, three-in-one.

Separation and purification of light hydrocarbons (LHs) are key industrial processes in petrochemical industries.[1,2] Modern industrialization and soaring global demand for natural gas and crude oil culminate in the ever-increasing demand for LH feedstock chemicals.[3,4] These commodity chemicals are regarded as high-value precursors to several manufactured commercial products, including plastics, fibers, and rubber.[5] Of particular importance is acetylene (C_2H_2) because it is one of the primary resources to manufacture plastics and several other industrially relevant organics, e.g., vinyl compounds, acrylic acid derivatives and α-ethynyl alcohols, *inter alia*.[6] The industrial manufacturing route to high-purity C_2H_2 often entails purifying it from a mixture of other small molecules, including methane (CH_4), carbon dioxide (CO_2) and ethylene (C_2H_4).

C_2H_2 is primarily produced from the incomplete combustion of methane and steam cracking of naphtha.[7] Further, C_2H_2 is identified as a major impurity in the industrial production of C_2H_4, poisoning the catalytic polymerization of C_2H_4 and eventually, resulting in the blockage of flammable gas flow-led explosions.[8] Of particular relevance is the development of porous by-design physisorbents with high LH separation efficiencies (C_2H_2/CO_2, C_2H_2/C_2H_4, C_2H_2/CH_4, etc.).[9] Generally, purification of LHs with close chemical and physical properties requires high-pressure and high-temperature conditions, culminating in unfavorably high energy penalties.[10−13] Traditional purification processes, such as high-cost extractions and distillations account for about 10−15% of the total global energy consumption. To exacerbate this current situation, global demand for these commodities is projected to triple by 2050.[14,15] Traditional purification methods such as partial hydrogenation and cryogenic distillation involve massive capital expenses and operational cost.[16,17] To mitigate these, physisorbents, such as metal−organic frameworks (MOFs), offer high upside potentials, because when designed right, low-cost recyclable MOFs have shown early signs of high cost-benefit ratios.[20−22] The right design of MOFs is prototypically controlled by the first-principles of crystal engineering (Scheme 1).

Scheme 1. Schematic Illustration Featuring the Prototypical Design of a MOF Functionalized with a Hemilabile Binding Site for C_2H_2[a]

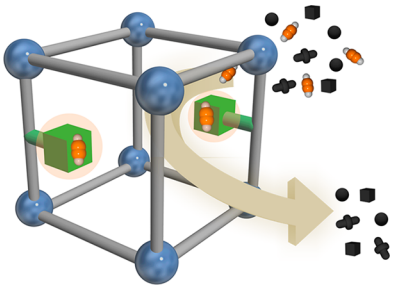

[a]This approach, if generalized, may lead to C_2H_2-selective advanced porous adsorbents.

In recent years, MOFs have sprung up as lead physisorbents for hydrocarbon selective adsorption. This primarily stems from their structural tunability, predesigned bottom-up architectures and long-range periodicity, thus guiding solid-state chemists to manifest control over their host−guest interactions.[18,19] With judicious choice of organic ligands and metal nodes, MOFs can be custom-designed to match up the sorbent prerequisites in the field of gas selectivity, of profound importance in the field of adsorptive separation and purification.[23−25] To this end, controlled surface functionalization and subångström level

Received: May 10, 2024
Revised: June 14, 2024
Accepted: June 18, 2024
Published: June 24, 2024

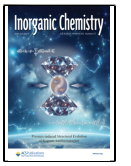

https://doi.org/10.1021/acs.inorgchem.4c01933
Inorg. Chem. 2024, 63, 12404−12408

precision of pore size control have transpired as the key factors to achieve high C_2H_2 separation/purification efficiency.[26] Thanks to amide groups inducing two distinct types of hydrogen bonding, amide-functionalized MOFs are particularly relevant. First, the -NH group can act as an electron acceptor, whereas the carbonyl is an electron donor; thus combining these can elicit weak coordinating sites that can reversibly coordinate and disconnect from the reactive metal coordination centers, thereby exemplifying hemilability.[27−29] Relying upon our in-house literature survey (see SI, Tables S4, S5), amide-functionalized MOFs are thus far unreported in the context hydrocarbon-selective adsorption of light hydrocarbon-selective adsorption.

Thanks to integrating all these aspects, particularly stemming from the hemilabile ligand *N*-(4*H*-1,2,4-triazol-4-yl)-isonicotinamide (L) (Scheme S2), here we introduce a previously unreported, three-dimensional (3D), ultramicroporous (pore size <7 Å) amide-functionalized MOF, $\{[Zn_2(L)(O)_2(DMF)].4DMF.3H_2O\}_n$ (DMF = *N*,*N*-dimethylformamide), hereinafter titled as **IPM-100** (IPM: IISER Pune Material). Single crystal structure of **IPM-100** was determined based on its crystallization in an orthorhombic $Pmn2_1$ space group (CCDC deposition 2338740). **IPM-100** was found to comprise two crystallographically distinguishable Zn(II) centers, Zn1 and Zn2 (Figure 1a) interconnected via a bridging

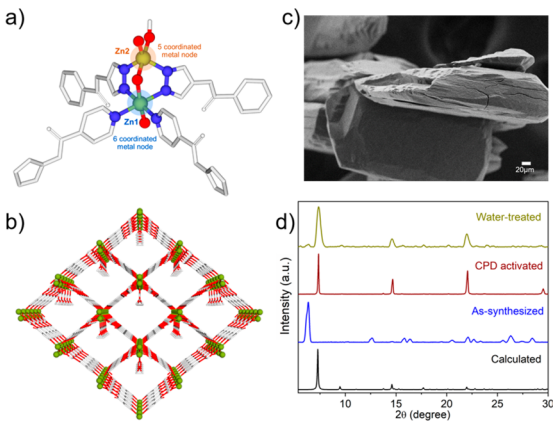

Figure 1. (a) Coordination environment of **IPM-100**. (b) Overall packing diagram of **IPM-100** along *c* axis. (c) FESEM image of **IPM-100**. (d) PXRD patterns of **IPM-100**.

oxygen atom. This bimetallic arrangement affords an oxo-bridged M-O-M chain propagating along the crystallographic *b* axis. Zn1 is hexacoordinated to four nitrogen atoms from four independent ditopic ligands (two ligands connected via the triazole end, and two ligands connected via the pyridine end) and two bridging oxygen molecules (Figure 1a). Conversely, the Zn2 site is pentacoordinated to two ligands (via the triazole N-termini), two bridging oxygens and one DMF solvent molecule (Figure 1a; Figures S4, S5). The asymmetric unit is comprised of two Zn(II) centers, a ligand (L), and one DMF molecule, each coordinated to Zn2 (Figure S4). The overall 3D MOF possesses 1D square channels along the *c* axis (Figure 1b; Figures S6−S8) with dimensions of 9.1 × 9.3 $Å^2$, elucidating the ultramicroporous nature of **IPM-100**. PLATON analysis indicated a void volume of 868 $Å^3$ (excluding guest solvent molecules), consistent with 45.4% of the guest-removed unit cell volume. Further, the crystal structure of **IPM-100** revealed a typical 6-connected **pcu** topology, a structural signature rather mainstream among thermodynamics-based MOF sorbents that exhibit gas separation.[32,33] Powder X-ray diffraction (PXRD) patterns indicate a slight shift to the characteristic peaks of **IPM-100**, whereas upon critical point drying (CPD) treatment,[34,35] the PXRD patterns revert to that of the pristine (Figure S9). This reversible change in PXRD patterns suggests a reversible structural transformation of **IPM-100**, induced by the guest solvent molecules solvating and desolvating in a two-way manner. Variable temperature PXRD diffractograms confirmed high polycrystallinity and structural integrity until 240 °C (Figure S10). Thermogravimetric (TGA) analysis of the as-synthesized **IPM-100** revealed the initial loss in weight percentage owing to the exclusion of the uncoordinated solvent molecules from the framework. CPD treatment was found to remove all the uncoordinated solvent molecules, a testament to the utility of this activation method (Figures S11, S12). Field emission scanning electron microscopy (FESEM) images of **IPM-100** crystals revealed rod shaped morphology, whereas elemental purity was substantiated from the FESEM based averaged elemental mapping spectra (Figure 1c; Figures S13−S15).

Cryogenic N_2 (77 K) and CO_2 (195 K) sorption isotherms were recorded with the activated **IPM-100**, with uptakes of ∼55 cm^3g^{-1} for N_2 and ∼185 cm^3g^{-1} for CO_2 was observed respectively (Figures S16, S17). Predicated upon the latter, the average internal pore diameter and Brunauer−Emmett−Teller (BET) surface area of **IPM-100** were found to be 7.5 Å (Figure S18) and 730.63 m^2g^{-1}, respectively (Figure S19).

That we could observe microporosity, a unison of multiple functionalities such as the presence of polar amide groups and nitrogen-rich Connolly surface in **IPM-100**, enthused us to explore its gas sorption properties. Interestingly, **IPM-100** registered high C_2H_2 saturation uptakes (at ∼1 bar) at both 298 K (∼77 cm^3g^{-1}) and 273 K (∼80 cm^3g^{-1}) (Figure 2a; Figure S20). Under identical conditions (298 K and 1 bar), considerably lower saturation uptakes were observed in other gas isotherms, viz., CO_2 (∼52 cm^3g^{-1}), C_2H_4 (∼24 cm^3g^{-1}) and CH_4 (∼4 cm^3g^{-1}) (Figure 2a; Figures S21−S23). This trend established **IPM-100** as a clear C_2H_2-selective adsorbent (Figure 2a). Akin to this ambient conditions' trend, **IPM-100** was found to be C_2H_2-selective at 273 K (Figures S20−S23). For C_2H_2, CO_2 and C_2H_4, the isosteric enthalpies of adsorption (Q_{st}) were determined by using the Virial expression on 273 and 298 K isotherms (Figures S24−S26). The low-coverage Q_{st} for C_2H_2, 39.5 $kJmol^{-1}$ was found to be significantly higher than that of CO_2 (21.4 $kJmol^{-1}$) and C_2H_4 (22.1 $kJmol^{-1}$) (Figures S27−S29). Favorable thermodynamics between C_2H_2 and **IPM-100** was evident from these differences in Q_{st}, $\Delta Q_{st})_{AC}$ ($(Q_{st})C_2H_2 - Q_{st}(CO_2)$) and $\Delta Q_{st})_{AE}$ ($(Q_{st})C_2H_2 - Q_{st}(C_2H_4)$), 18.1 and 17.4 $kJmol^{-1}$, respectively. Such high $\Delta Q_{st} > 15$ $kJmol^{-1}$ is a key parameter to achieve efficient binary separation (Tables S4, S5). The ΔQ_{st} for **IPM-100** was found to stand among the higher values reported in the MOF-literature (Figures 2b, 2c). Further, a clear difference between adsorption capacities under separation-relevant partial pressures at 298 K indicate the sorbent's potential to exhibit high C_2H_2 selectivity and uptake driven C_2H_2/CO_2, C_2H_2/C_2H_4, and $C_2H_2/CO_2/C_2H_4$ separations (Figures S27−30), a combination that remains rare among physisorbents.[36] **IPM-100** exhibited a strong C_2H_2 uptake of ∼59 cm^3g^{-1} under low pressure of 0.25 bar, whereas the corresponding CO_2 and C_2H_4 uptakes were found to be low, 14 and 11.5 cm^3g^{-1}, respectively (Figures S31−S33). Such a significant difference in adsorption isotherms and the corre-

https://doi.org/10.1021/acs.inorgchem.4c01933
Inorg. Chem. 2024, 63, 12404−12408

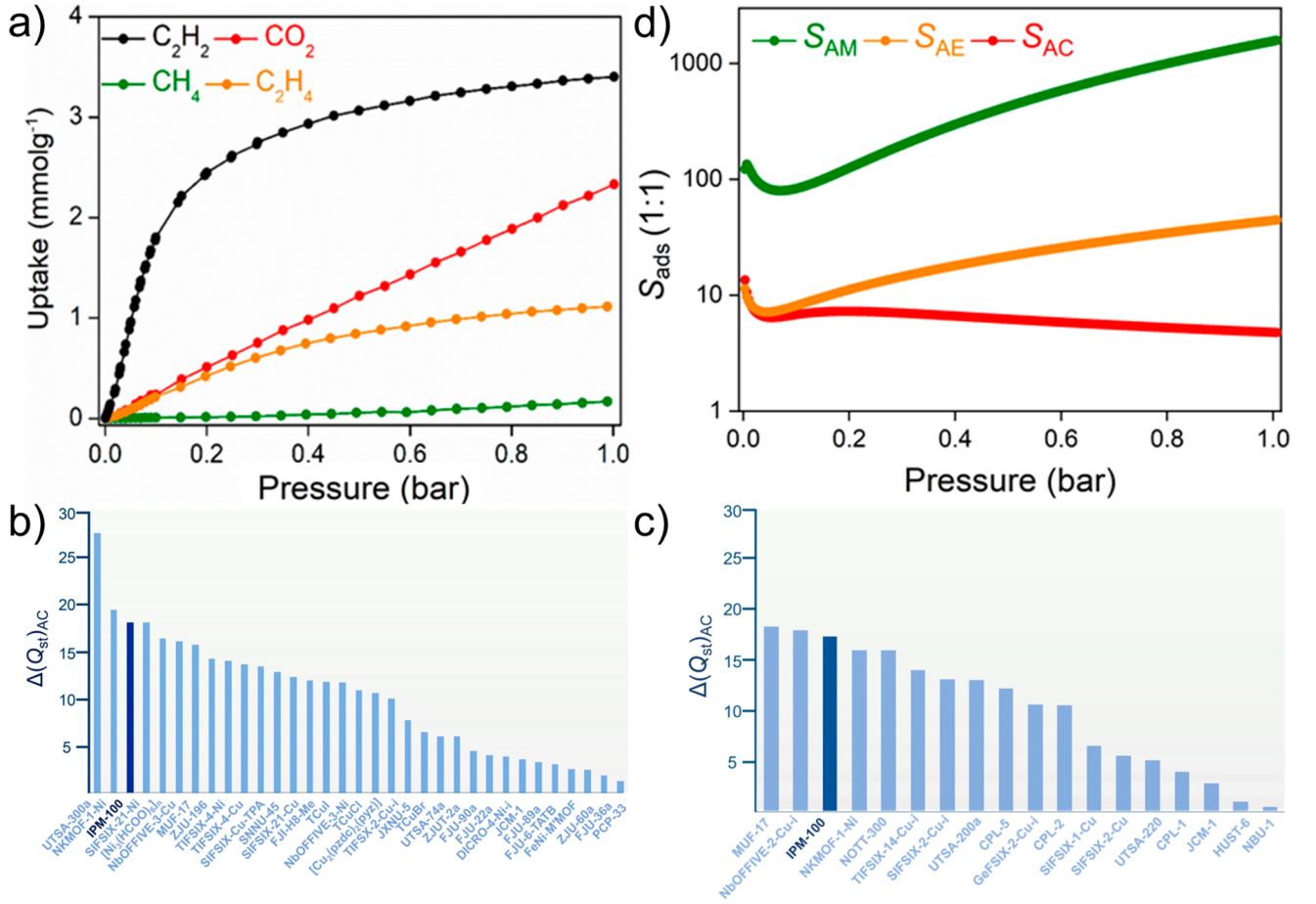

Figure 2. (a) Single-component light hydrocarbon and CO_2 adsorption isotherms at 298 K by **IPM-100**. Comparison between (b) $(\Delta Q_{st})_{AC}$ values. (c) $(\Delta Q_{st})_{AE}$ for **IPM-100** with other top-performing MOF sorbents that exhibit C_2H_2/CO_2 and C_2H_2/C_2H_4 selectivities. (d) IAST selectivity by **IPM-100** of C_2H_2/CO_2, C_2H_2/C_2H_4, and C_2H_2/CH_4 mixtures (1/1, v/v).

sponding adsorption enthalpies suggest a clear C_2H_2 selectivity over CO_2, CH_4 and C_2H_4.

Ideal adsorbed solution theory (IAST) was applied to evaluate the adsorption selectivities for C_2H_2 from three different binary mixtures of equimolar (1/1, v/v) compositions, C_2H_2/CO_2, C_2H_2/C_2H_4 and C_2H_2/CH_4 (Figure 2d; Figure S34; Table S2). The determined selectivities were found to be as high as 5 (C_2H_2/CO_2), 45 (C_2H_2/C_2H_4) and 1600 (C_2H_2/CH_4), at 298 K and 1 bar. These selectivities, in tandem with high $\Delta(Q_{st})_{AC}$ and $\Delta(Q_{st})_{AE}$ imply that IPM-100 is in the same league as some of the best-performing C_2H_2 selective MOF benchmarks (Tables S4, S5).

To examine the combined merits of uptake capacity and sorption selectivity in translating **IPM-100** to fixed-bed dynamic column-based breakthrough separation performances, several simulated breakthrough experiments were conducted at 298 K (Scheme S1, Figure S35). A fixed adsorbent bed comprised of 0.3 g of **IPM-100** was used following a literature-reported protocol (see SI for details; Table S3, Figures S35, S36).[30,31] Equimolar hydrocarbon mixtures were introduced as feeds to mimic a range of industrial process conditions. As evident in the Figure S35a–c, the other LHs, i.e., C_2H_4, CH_4 and CO_2 broke through first from the **IPM-100** bed whereas the retention of C_2H_2 within the bed continued for a significant time until C_2H_2 reached its saturation to break through. Such high retention performance is indicative of strong preferential binding of C_2H_2 with **IPM-100** and reflects a likelihood of the compound's translation into higher technological readiness levels, vis-à-vis C_2H_2/C_2H_4, C_2H_2/CO_2, and C_2H_2/CH_4 separations, contingent on further success with experimental validation.

Density functional theory (DFT) calculations and Canonical Monte Carlo (CMC) simulations were performed to shed light on the preferred framework state and adsorption binding sites (see SI for details). The atomic positions of **IPM-100** molecular models were DFT-optimized at the experimentally refined cell parameters for different models (see Figure 3a, and supplementary structures as SI). Only the form with deprotonated ligand (L) and fully protonated oxide chain (Zn–OH–Zn–OH–) revealed stability during optimization, maintaining all the Zn–N interactions <2.4 Å. In contrast to the other forms with neutral ligand forms (amide or iminol) or even with partially deprotonated ligands (Figure 3a), some of the Zn–N interactions optimized to distances over 3 Å. This led to ligand detachment from the Zn-oxide chain.

Predicated upon the most stable DFT-optimized **IPM-100** model, and relying on CMC simulations at a fixed loading of 1 molecule per 2 × 2 × 2 supercell, the most plausible binding sites for CH_4, CO_2, C_2H_2, and C_2H_4 were determined. The results are visualized as the adsorbates' density fields (Figures S42–S45) and the corresponding occupational isosurfaces (Figures S46–S49). Coordinates for the most stable DFT-optimized binding sites can be visualized together with the binding site isosurfaces derived from the CMC simulations, as shown in Figures S46–S49. In their most stable DFT binding sites, the adsorption

https://doi.org/10.1021/acs.inorgchem.4c01933
Inorg. Chem. 2024, 63, 12404–12408

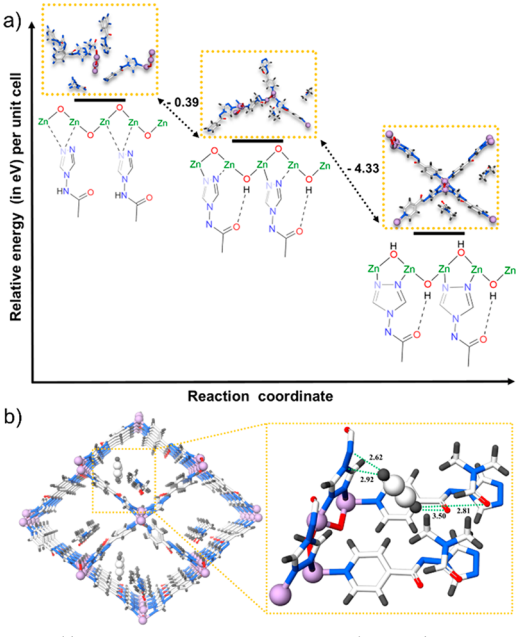

Figure 3. (a) Relative energy diagram for the **IPM-100** forms (left to right): the regular amide form, the form with 50% iminol and 50% deprotonated L (bearing protonated ZnO chain), and the fully deprotonated ligand (bearing Zn−OH−Zn−OH chain) form. (b) The most plausible DFT-optimized C_2H_2 binding site.

enthalpies at 298 K are −27.6 (CH_4), −38.3 (C_2H_4), −44.4 (CO_2) and −51.5 (C_2H_2) kJmol^{-1}, a trend consistent with our experimental findings. The C_2H_2-selective interactions comprise its favorable interactions with the hemilabile ligand's triazole and pyridine rings. These are further strengthened by H(C_2H_2)-N(L) interactions (2.62 and 2.92 Å), whereas the other hydrogen of C_2H_2 cooperatively interacts with O atoms from DMF (2.81 Å) and L (3.50 Å) (Figure 3b and Figure S37).

In conclusion, we report a hemilabile *N*-donor ligand self-assembling to deliver an amide-functionalized new MOF, **IPM-100**. Thanks to its hemilabile nature of binding sites, **IPM- 100** can adopt configurations that exhibit strong C_2H_2 selectivity over three similar-sized gases concurrently under ambient conditions, C_2H_4, CO_2, and CH_4. While in general the presence of guest solvent molecules such as DMF partially blocking the pore is considered a nemesis in prototypical MOFs,[37] we leverage this aspect of **IMP-100** to our favor in the DMF-coordinated activated phase. This work introduces a new approach to design ultramicroporous (pore diameter <7 Å) and supermicroporous (pore diameter >7 Å) coordination networks in the context of selective gas adsorption driven commodity chemical purifications, including but not limited to the energy-efficient separation of light hydrocarbon molecules.

■ ASSOCIATED CONTENT

Data Availability Statement

The data that support these findings are available upon reasonable request to the authors.

Supporting Information

The Supporting Information is available free of charge at https://pubs.acs.org/doi/10.1021/acs.inorgchem.4c01933.

Details of the materials and methods, synthesis and characterization of IPM-100 including crystallographic data, crystal structure, PXRD patterns, TGA curves, FESEM images, gas adsorption curves, and theoretical calculations (PDF)

Accession Codes

CCDC 2338740 contains the supplementary crystallographic data for this paper. These data can be obtained free of charge via www.ccdc.cam.ac.uk/data_request/cif, or by emailing data_request@ccdc.cam.ac.uk, or by contacting The Cambridge Crystallographic Data Centre, 12 Union Road, Cambridge CB2 1EZ, UK; fax: +44 1223 336033.

■ AUTHOR INFORMATION

Corresponding Authors

Tarak Nath Mandal − *Department of Chemistry, Indian Institute of Science Education and Research (IISER), Pune 411008, India; Department of Chemistry, SRM Institute of Science and Technology, Kattankulathur, Tamil Nadu 603203, India*; Phone: +91 20 2590 8076; Email: mandaltaraknathchemi@gmail.com

Sujit K. Ghosh − *Department of Chemistry, Indian Institute of Science Education and Research (IISER), Pune 411008, India*; orcid.org/0000-0002-1672-4009; Email: sghosh@iiserpune.ac.in

Matthias Vandichel − *Department of Chemical Sciences, Bernal Institute, University of Limerick, Castletroy, Limerick V94 T9PX, Ireland*; orcid.org/0000-0003-1592-0726; Email: matthias.vandichel@ul.ie

Authors

Subhajit Dutta − *Department of Chemistry, Indian Institute of Science Education and Research (IISER), Pune 411008, India*; orcid.org/0000-0003-1440-7808

Soumya Mukherjee − *Department of Chemical Sciences, Bernal Institute, University of Limerick, Castletroy, Limerick V94 T9PX, Ireland*; orcid.org/0000-0003-2375-7009

Sousa Javan Nikkhah − *Department of Chemical Sciences, Bernal Institute, University of Limerick, Castletroy, Limerick V94 T9PX, Ireland*; orcid.org/0000-0003-1725-4069

Omid T. Qazvini − *Svante Inc., Burnaby, BC V5J 5K3, Canada*

Gourab K. Dam − *Department of Chemistry, Indian Institute of Science Education and Research (IISER), Pune 411008, India*; orcid.org/0000-0001-6130-4559

Complete contact information is available at: https://pubs.acs.org/10.1021/acs.inorgchem.4c01933

Author Contributions

⊥S.D. and S.M. contributed equally. All authors have given approval to the final version of the manuscript.

Notes

The authors declare no competing financial interest.

■ ACKNOWLEDGMENTS

S.D. and S.K.G. thank IISER Pune and SERB (Project No. CRG/2022/001090) for research funding. S.M. acknowledges an SFI-IRC Pathway award (21/PATH-S/9454) from the Science Foundation Ireland. S.J.N. and M.V. acknowledge the Irish Center for High-End Computing (ICHEC). S.J.N. thanks Enterprise Ireland and the European Union's Horizon 2020 research and innovation programme under the Marie Skłodowska-Curie grant agreement 847402 (ID: MF20210297).

REFERENCES

(1) Yang, S.; Ramirez-Cuesta, A. J.; Newby, R.; Garcia-Sakai, V.; Manuel, P.; Callear, S. K.; Campbell, S. I.; Tang, C. C.; Schröder, M. Supramolecular binding and separation of hydrocarbons within a functionalized porous metal−organic framework. *Nat. Chem.* **2015**, *7*, 121−129.

(2) Bao, Z.; Chang, G.; Xing, H.; Krishna, R.; Ren, Q.; Chen, B. Potential of microporous metal-organic frameworks for separation of hydrocarbon mixtures. *Energy Environ. Sci.* **2016**, *9*, 3612−3641.

(3) Sholl, D. S.; Lively, R. P. Seven chemical separations to change the world. *Nature* **2016**, *532*, 435−437.

(4) Peplow, M. Materials Science: The Hole Story. *Nature* **2015**, *520*, 148−150.

(5) Ren, T.; Patel, M.; Blok, K. Olefins from Conventional and Heavy Feedstocks: Energy use in Steam Cracking and Alternative Processes. *Energy* **2006**, *31*, 425−451.

(6) P-ssler, P.; Hefner, W.; Buckl, K.; Meinass, H.; Wernicke, H.-J.; Ebersberg, G.; Mgller, R.; B-ssler, J.; Behringer, H.; Mayer, D. *Ullmann's Encyclopedia of Industrial Chemistry*; Wiley-VCH, Weinheim, 2000.

(7) Yang, L.; Qian, S.; Wang, X.; Cui, X.; Chen, B.; Xing, H. Energy-efficient separation alternatives: metal-organic frameworks and membranes for hydrocarbon separation. *Chem. Soc. Rev.* **2020**, *49*, 5359−5406.

(8) Li, H.; Li, L.; Lin, R.-B.; Ramirez, G.; Zhou, W.; Krishna, R.; Zhang, Z.; Xiang, S.; Chen, B. Microporous Metal-Organic Framework with Dual Functionalities for Efficient Separation of Acetylene from Light Hydrocarbon Mixtures. *ACS Sustainable Chem. Eng.* **2019**, *7*, 4897−4902.

(9) Barnett, B. R.; Gonzalez, M. I.; Long, J. R. Recent progress towards light hydrocarbon separations using metal−organic frame-works. *Trends in Chem.* **2019**, *1* (2), 159−171.

(10) Zhang, X.; Li, L.; Wang, J.-X.; Wen, H.-M.; Krishna, R.; Wu, H.; Zhou, W.; Chen, Z.-N.; Li, B.; Qian, G.; Chen, B. Selective ethane/ethylene separation in a robust microporous hydrogen-bonded organic framework. *J. Am. Chem. Soc.* **2020**, *142*, 633−640.

(11) Li, J.; Jiang, L.; Chen, S.; Kirchon, A.; Li, B.; Li, Y.; Zhou, H.-C. Metal−organic framework containing planar metal-binding sites: efficiently and cost-effectively enhancing the kinetic separation of C_2H_2/C_2H_4. *J. Am. Chem. Soc.* **2019**, *141*, 3807−3811.

(12) Dutta, S.; Mukherjee, S.; Qazvini, O. T.; Gupta, A. K.; Sharma, S.; Mahato, D.; Babarao, R.; Ghosh, S. K. Three-in-One C2H2-Selectivity-Guided Adsorptive Separation across an Isoreticular Family of Cationic Square-Lattice MOFs. *Angew. Chem., Int. Ed.* **2022**, *61*, No. e202114132.

(13) Sharma, S.; Mukherjee, S.; Desai, A. V.; Vandichel, M.; Dam, G. K.; Jadhav, A.; Kociok-Köhn, G.; Zaworotko, M. J.; Ghosh, S. K. Efficient Capture of Trace Acetylene by an Ultramicroporous Metal−Organic Framework with Purine Binding Sites. *Chem. Mater.* **2021**, *33*, 5800−5808.

(14) Chen, K.-J.; Madden, D. G.; Mukherjee, S.; Pham, T.; Forrest, K. A.; Kumar, A.; Space, B.; Kong, J.; Zhang, Q.-Y.; Zaworotko, M. J. Synergistic sorbent separation for one-step ethylene purification from a four-component mixture. *Science* **2019**, *366* (6462), 241−246.

(15) Wang, Z.; Zhang, S.; Chen, Y.; Zhang, Z.; Ma, S. Covalent organic frameworks for separation applications. *Chem. Soc. Rev.* **2020**, *49* (3), 708−735.

(16) Sun, F.-Z.; Yang, S.-Q.; Krishna, R.; Zhang, Y.-H.; Xia, Y.-P.; Hu, T.-L. Microporous metal−organic framework with a completely reversed adsorption relationship for C2 hydrocarbons at room temperature. *ACS Appl. Mater. Interfaces* **2020**, *12*, 6105−6111.

(17) Krishnaraj, C.; Jena, H.; Leus, K.; Freeman, H.; Benning, L.; Van der Voort, P. An Aliphatic Hexene-Covalent Triazine Framework for Selective Acetylene/Methane and Ethylene/Methane Separation. *J. Mater. Chem. A* **2019**, *7*, 13188−13196.

(18) Kuppler, R. J.; Timmons, D. J.; Fang, Q.-R.; Li, J.-R.; Makal, T. A.; Young, M. D.; Yuan, D.; Zhao, D.; Zhuang, W.; Zhou, H.-C. Potential Applications of Metal-Organic Frameworks. *Coord. Chem. Rev.* **2009**, *253*, 3042−3066.

(19) Bobbitt, N. S.; Mendonca, M. L.; Howarth, A. J.; Islamoglu, T.; Hupp, J. T.; Farha, O. K.; Snurr, R. Q. Metal−Organic Frameworks for the Removal of Toxic Industrial Chemicals and Chemical Warfare Agents. *Chem. Soc. Rev.* **2017**, *46*, 3357−3385.

(20) Tian, D.; Xu, J.; Xie, Z.-J.; Yao, Z.-Q.; Fu, D.-L.; Zhou, Z.; Bu, X.-H. The first example of hetero-triple-walled metal−organic frameworks with high chemical stability constructed via flexible integration of mixed molecular building blocks. *Adv. Sci.* **2016**, *3*, 1500283.

(21) Dutta, S.; More, Y. D.; Fajal, S.; Mandal, W.; Dam, G. K.; Ghosh, S. K. Ionic metal−organic frameworks (iMOFs): progress and prospects as ionic functional materials. *Chem. Commun.* **2022**, *58*, 13676−13698.

(22) Yuan, S.; Feng, L.; Wang, K.; Pang, J.; Bosch, M.; Lollar, C.; Sun, Y.; Qin, J.; Yang, X.; Zhang, P.; Wang, Q.; Zou, L.; Zhang, Y.; Zhang, L.; Fang, Y.; Li, J.; Zhou, H.-C. Stable metal−organic frameworks: Design, synthesis, and applications. *Adv. Mater.* **2018**, *30*, 1704303.

(23) Mukherjee, S.; Sensharma, D.; Qazvini, O. T.; Dutta, S.; Macreadie, L. K.; Ghosh, S. K.; Babarao, R. Advances in Adsorptive Separation of Benzene and Cyclohexane by Metal-Organic Frame-work Adsorbents. *Coord. Chem. Rev.* **2021**, *437*, 213852.

(24) Dong, Q.; Guo, Y.; Cao, H.; Wang, S.; Matsuda, R.; Duan, J. Accelerated C2H2/CO2 Separation by a Se-Functionalized Porous Coordination Polymer with Low Binding Energy. *ACS Appl. Mater.Interfaces2020* **2020**, *12*, 3764−3772.

(25) Lin, R.-B.; Xiang, S.; Zhou, W.; Chen, B. Microporous Metal-Organic Framework Materials for Gas Separation. *Chem.* **2020**, *6*, 337−363.

(26) Lin, R. B.; Xiang, S.; Xing, H.; Zhou, W.; Chen, B. Exploration of Porous Metal−Organic Frameworks for Gas Separation and Purification. *Coord. Chem. Rev.* **2019**, *378*, 87−103.

(27) Chen, Z.; Liu, Z.; Xu, X. Dynamic evolution of the active center driven by hemilabile coordination in Cu/CeO2 single-atom catalyst. *Nat. Commun.* **2023**, *14*, 2512.

(28) Adams, G. M.; Weller, A. S. POP-type ligands: Variable coordination and hemilabile behaviour. *Coord. Chem. Rev.* **2018**, *355*, 150−172.

(29) Slone, C. S.; Weinberger, D. A.; Mirkin, C. A. Transition Metal Coordination Chemistry of Hemilabile Ligands. *Progress in Inorganic Chemistry* **1999**, *48*, 233.

(30) Qazvini, O. T.; Telfer, S. G. A Robust Metal-Organic Framework for Post-Combustion Carbon Dioxide Capture. *J. Mater. Chem. A* **2020**, *8*, 12028−12034.

(31) Tohidi, Z.; Fatemi, S.; Qazvini, O. T. Mercaptan Removal from Natural Gas by the Efficient Cyclic Adsorption Process; a Simulation Study. *J. Nat. Gas Sci. Eng.* **2015**, *26*, 758−769.

(32) Bhatt, P. M.; Guillerm, V.; Datta, S. J.; Shkurenko, A.; Eddaoudi, M. Topology Meets Reticular Chemistry for Chemical Separations: MOFs as a Case Study. *Chem.* **2020**, *6*, 1613−1633.

(33) Mukherjee, S.; Champness, N. R. Tiny pores turning the tide. *Nat. Rev. Chem.* **2024**, *8*, 6−7.

(34) Nelson, A. P.; Farha, O. K.; Mulfort, K. L.; Hupp, J. T. Supercritical Processing as a Route to High Internal Surface Areas and Permanent Microporosity in Metal−Organic Framework Materials. *J. Am. Chem. Soc.* **2009**, *131*, 458−460.

(35) Liu, B.; Wong-Foy, A. G.; Matzger, A. J. Rapid and enhanced activation of microporous coordination polymers by flowing supercritical CO_2. *Chem. Commun.* **2013**, *49*, 1419−1421.

(36) Harvey-Reid, N. C.; Sensharma, D.; Mukherjee, S.; Patil, K. M.; Kumar, N.; Nikkhah, S. J.; Vandichel, M.; Zaworotko, M. J.; Kruger, P. E. Crystal Engineering of a New Hexafluorogermanate Pillared Hybrid Ultramicroporous Material Delivers Enhanced Acetylene Selectivity. *ACS Appl. Mater. Interfaces* **2024**, *16* (4), 4803−4810.

(37) Feldblyum, J. I.; Liu, M.; Gidley, D. W.; Matzger, A. J. Reconciling the Discrepancies between Crystallographic Porosity and Guest Access As Exemplified by Zn-HKUST-1. *J. Am. Chem. Soc.* **2011**, *133*, 18257−18263.

https://doi.org/10.1021/acs.inorgchem.4c01933
Inorg. Chem. 2024, 63, 12404−12408